



Lawrence Berkeley Laboratory

UNIVERSITY OF CALIFORNIA

Materials & Molecular Research Division

Submitted to Engineering Fracture Mechanics

MICROMECHANISMS OF FATIGUE CRACK GROWTH
RETARDATION FOLLOWING OVERLOADS

S. Suresh

May 1982

RECEIVED
LAWRENCE
BERKELEY LABORATORY

JUL 15 1982

LIBRARY AND
DOCUMENTS SECTION

TWO-WEEK LOAN COPY

*This is a Library Circulating Copy
which may be borrowed for two weeks.
For a personal retention copy, call
Tech. Info. Division, Ext. 6782.*



LBL-14482
c.2

DISCLAIMER

This document was prepared as an account of work sponsored by the United States Government. While this document is believed to contain correct information, neither the United States Government nor any agency thereof, nor the Regents of the University of California, nor any of their employees, makes any warranty, express or implied, or assumes any legal responsibility for the accuracy, completeness, or usefulness of any information, apparatus, product, or process disclosed, or represents that its use would not infringe privately owned rights. Reference herein to any specific commercial product, process, or service by its trade name, trademark, manufacturer, or otherwise, does not necessarily constitute or imply its endorsement, recommendation, or favoring by the United States Government or any agency thereof, or the Regents of the University of California. The views and opinions of authors expressed herein do not necessarily state or reflect those of the United States Government or any agency thereof or the Regents of the University of California.

MICROMECHANISMS OF FATIGUE CRACK GROWTH
RETARDATION FOLLOWING OVERLOADS

by

S. Suresh
Department of Materials Science and Mineral Engineering
and Materials and Molecular Research Division of
Lawrence Berkeley Laboratory
University of California
Berkeley, California 94720

May 1982

Submitted for publication in Engineering Fracture Mechanics

This work was supported by the Director, Office of Energy Research,
Office of Basic Energy Sciences, Materials Science Division of the
U.S. Department of Energy under Contract No. DE-AC03-76SF00098.

Micromechanisms of Fatigue Crack Growth

Retardation Following Overloads

S. Suresh

Department of Materials Science and Mineral Engineering
and Materials and Molecular Research Division of
Lawrence Berkeley Laboratory
University of California
Berkeley, California 94720

Abstract

New mechanistic interpretations to rationalize fatigue crack growth retardation due to load excursions are presented. It is reasoned that crack closure arising from residual tensile displacements is not the *primary* mechanism for growth attenuation following a peak tensile overload. A new mechanism for retardation is discussed in terms of a "micro-roughness" model. Quantitative analyses are provided to estimate the extent of reductions in *effective* driving force in the retarded growth region due to possible crack branching, residual compressive stresses and fracture face micro-roughness. It is argued that the retarded crack advance is *effectively* governed by the micromechanisms of Stage I growth although *nominally* Stage II conditions exist in the post-overload zone. The implications of the present arguments are shown to be consistent with a number of typical post-overload phenomena cited in the literature.

NOTATION

a	= crack length
a^*	= total retarded crack growth distance
a_d	= delay distance (retarded crack advance up to the lowest growth rate)
$(da/dN)_B$	= baseline crack propagation rate
$(da/dN)_R$	= retarded crack propagation rate
h	= average asperity height
H	= height of the specimen
k	= effective stress intensity factor for branched crack
k_1	= Mode I stress intensity factor for branched crack
K_1	= Mode I stress intensity factor for main crack
k_2	= Mode II stress intensity factor for branched crack
K_2	= Mode II stress intensity factor for main crack
K_{c1}	= closure stress intensity factor
$K_{c1,MR}$	= closure stress intensity factor accounting for asperity contact
K_{1max}	= baseline maximum stress intensity factor
K_{2max}	= overload maximum stress intensity factor
K_{1min}	= baseline minimum stress intensity factor
K_{IR}	= stress intensity factor due to residual stress field
$K_{IR,B}$	= value of K_{IR} during baseline (pre-overload) crack growth
$K_{IR,OL}$	= value of K_{IR} following an overload
N^*	= number of cycles for retarded crack growth
r_c	= cyclic plastic zone size
r_{OL}	= overload factor ($= K_{2max}/K_{1max}$)
R	= nominal baseline load ratio ($= K_{1min}/K_{1max}$)
$R_{Cr,B}$	= critical value of R for baseline crack growth
$R_{Cr,OL}$	= critical value of R for the effect of enlarged residual stress field
U_I	= Mode I crack displacement
U_{II}	= Mode II crack displacement
w	= average asperity base width
x	= ratio of Mode I and Mode II displacements ($= U_I/U_{II}$)
α	= angle denoting the extent of the second kink for doubly-kinked cracks

γ	= non-dimensional surface roughness parameter (= h/w)
δ_{c1}	= crack tip opening displacement at first asperity contact
δ_{1max}	= crack tip opening displacement at K_{1max}
δ_{1min}	= crack tip opening displacement at K_{1min}
ΔK_B	= baseline stress intensity factor range
ΔK_{eff}	= effective stress intensity factor range
$[\Delta K_{eff}]_{MR}$	= value of ΔK_{eff} accounting for fracture face micro-roughness
$[\Delta K_{eff}]_{R,B}$	= value of ΔK_{eff} accounting for residual stresses during baseline crack growth
$[\Delta K_{eff}]_{R,OL}$	= value of ΔK_{eff} accounting for residual stresses generated by an overload
ΔK_0	= threshold stress intensity factor range
ΔK_{OL}	= overload stress intensity factor range
$[\Delta K_{red}]_{R,OL}$	= excess reduction in ΔK_{eff} due to enlarged residual stress field
κ_{ij}	= constants relating k_1 , k_2 , K_1 and K_2
ψ	= asperity semi-cone angle
ρ	= distance over which residual compressive stresses are active
σ_0	= flow stress
σ_R	= residual stress
θ	= angle denoting the extent of first branch or kink

1. INTRODUCTION

It is now experimentally well documented that during fatigue crack growth, load excursions in the form of single tensile overloads or high-low block loading sequences result in crack growth retardation or arrest. Although the transient effects accompanying load interactions are of paramount importance in the prediction of fatigue life and inspection intervals in such applications as proof testing of pressure vessels or overspeed testing of rotating machinery, the micromechanisms governing the retardation phenomena are not yet clearly understood. Currently available mechanistic arguments to account for growth transients involve concepts based on a) crack closure due to residual plastic deformation in the wake of the advancing crack front (1-3), b) crack tip blunting (4,5), c) residual compressive stresses close to the crack tip (6,7) and the accompanying interactions between the crack tip and the elastic/plastic boundary (8,9) and d) possible crack tip strain hardening (10,11). Although existing experimental information from numerous investigations clearly indicates that a single mechanism may not completely govern the complex transient behavior following load excursions, contributions to the retardation phenomenon due to different mechanistic possibilities have thus far not been well characterized.

In the present paper, the possible role of various mechanistic processes in controlling growth attenuation is critically examined. Although a large body of evidence indicates that the phenomenon of crack closure (11-15) and the extent of plastic zone directly ahead of the crack tip (5) are of more significance under plane stress conditions, experimental results for a low strength steel are presented

to demonstrate that complete crack arrest can occur due to an overload under plane strain conditions. Simple quantitative analyses are carried out to estimate the contributions to growth attenuation arising from residual compressive stresses and possible crack branching following overloads. A new mechanism for enhanced retardation (16) is suggested in terms of a "micro-roughness" model. It is shown that several well documented post-overload phenomena can be rationalized in terms of the present mechanistic interpretations. Although attention is focussed primarily on transient effects following a single overload (in order to identify and analyze clearly the underlying mechanisms), other types of load interactions are also briefly discussed. The implications of the proposed arguments are described not only from a mechanistic viewpoint, but also in terms of the measurement of crack growth rates, especially at low stress intensities.

2. EVALUATION OF PREVIOUS MODELS

Fig. 1 schematically shows typical crack growth retardation behavior following load interaction in the form of a peak tensile overload. During fatigue crack growth at a baseline stress intensity range $\Delta K_B (= K_{I_{max}} - K_{I_{min}})$, the application of a single overload (Fig. 1a) results in a reduction in crack propagation rate from a baseline value of $(da/dN)_B$ to $(da/dN)_R$, with the lowest growth rate occurring over a delay distance a_d , as shown in Fig. 1b. The retarded crack propagates over a total distance of a^* (for N^* cycles after an overload) before the growth rates catch up with the pre-overload baseline values.

Numerous investigators (6,8,17,18) have employed arguments based on residual compressive stresses at or close to the crack tip and the accompanying yield zone interactions to explain retardation subsequent to overload cycling. Such stresses arise as a result of the elastic unloading of the sample which clamps the enlarged cyclic plastic zone generated by the overload to produce a residual compressive stress field at the tip of the crack (5).

Wheeler (8) suggested a semi-empirical model based on the premise that retardation occurs because the crack has to traverse through the overload plastic zone. The extent of retardation is therefore related to the distance the retarded crack has advanced in the plastic zone. Willenborg et al (9) presented an alternative model based on the assumption that the stress intensity $K_{I_{max}}$ actually occurring at the current crack length will be effectively reduced due to residual stresses. The decrease in stress intensity is proportional to the square root of the distance the crack has to propagate to be free of the residual stresses arising from an overload.

The semi-empirical engineering models by Wheeler (8) and Willenborg et al (9) require the crack growth attenuation to be immediate after an overload and do not allow for delayed retardation which has been experimentally observed. The discontinuity in crack growth rates at the point of application of an overload (as predicted by these models) illustrates the absence of realistic mechanisms for retardation. Moreover, several typical post-overload observations on microstructural effects (3) cannot be easily rationalized by means of such simple engineering models. In addition, while residual compressive stresses are

known to play a major role in reducing effective stress intensity values over distances of the order of the reversed plastic zone size (5) due to the overload, the retarded crack growth distance could be up to an order of magnitude larger than the extent of the reversed plastic zone directly ahead of the crack tip (19-21), especially under plane strain conditions. Thus, it appears that although residual compressive stresses constitute a major and viable mechanism for retardation following an overload, they cannot *solely* account for several post-overload observations.

While the residual compressive stresses are generally considered to play a dominant role *at or close to* the crack tip, Elber (1,2) suggested that the permanent residual tensile displacements formed due to plastic deformation could result in contact between the fracture surfaces in the *wake* of the advancing crack front, even at tensile loads. Since the crack cannot propagate while it remains closed, the effective stress intensity range, ΔK_{eff} , responsible for crack growth is given by

$$\Delta K_{eff} = K_{lmax} - K_{cl} \quad (1)$$

where K_{lmax} and K_{cl} are the maximum and closure stress intensities, respectively, during cyclic loading. Such (plasticity-induced) crack closure arguments have been used to explain the transient effects following single as well as high-low block overloads (1-3, 22-24). Extensive fractographic studies of overload effects in 2024-T3 aluminum alloy by von Euw and Hertzberg (3,23) typically showed pre-overload crack advanced by Stage II (in Forsyth's terminology (25)) striation crack advance, stretch zone due to the application of a single overload

and highly abraded post-overload zone with irregular surface features and no discernable striations. Such abraded and striationless post-overload crack growth has been observed by a number of researchers for a wide range of alloys and overload ratios (3,17,22-24, 26-29), except in situations where the extent of retardation is small in comparison to the baseline propagation rates (22). Based on Elber's (plasticity-induced) crack closure arguments, von Ew et al (3) suggested that the enhanced residual plastic deformation arising from the overload cycle results in crack face contact in the *wake* of the advancing crack tip which accounts for not only the retarded crack growth but also delayed retardation. However, information on attenuated crack growth from a number of studies (19-21, 30-32) reveals that such crack closure processes cannot fully explain the transient effects due to load excursions. An examination of crack tip profiles following overloads indicates the crack is severely blunted by the spike tensile overload (16,33,35). Such blunting, which persists for several cycles following an overload, suggests that plasticity-induced crack closure in the wake of the crack does not play a major role in retardation (16,33,35). (In fact, severe blunting following an overload removes the crack closure which exists during pre-overload cycling and is consistent with some observations of accelerated crack advance for a few cycles immediately following an overload (26)). While it is well established that plasticity-induced crack closure can occur during Stage II plane stress constant amplitude loading without any abrasion marks or obliteration of striations (1,2,28), it is inconceivable that the same mechanism of crack closure can remove the striation marks on the fracture

surface by an abrasion process (3) or enhance microstructure-sensitivity in the post-overload zone. In addition, there is existing experimental evidence indicating that plasticity-induced crack closure due to residual tensile displacements in the wake of the crack plays a more important role under *plane stress* conditions (11-15). Yet, considerable crack growth retardation does occur following single overloads at lower ΔK levels where predominantly *plane strain* conditions exist (19-22). Thus, it is inferred that although plasticity-induced crack closure in the wake of the crack can occur in plane stress constant amplitude and high-low block tensile overload situations, it does not appear to be a *primary* mechanism for retardation following single overloads.

It can be argued that crack tip strain hardening and blunting are also not the governing mechanisms for growth attenuation. Jones reported that pre-strain hardening accelerates, rather than retard, crack propagation rates (10). Although blunting does occur on overload cycling (4,5), it cannot be the primary mechanism for retardation since the retarded crack branches away from the blunted main crack through the shear bands generated by the overload (19).

3. MICROMECHANISMS OF CRACK GROWTH RETARDATION

Possible mechanisms for crack growth retardation arising from a single overload are described in the following sections. Mechanical models are presented to estimate roughly the extent of reduction in ΔK_{eff} due to each mechanism.

Fig. 2 shows the sequential changes in crack tip profile in a 6061-T6 aluminum alloy due to a single overload ($r_{OL} = 1.8$) applied at a baseline stress intensity range of $\Delta K_B = 10 \text{ MPa}\sqrt{\text{m}}$, from the work

of Lankford and Davidson (33). It is obvious from Figs. 2a and 2b that the overload severely blunts the crack tip and produces intense shear bands. Fig. 2c and similar results in other alloy systems (19,29,33,34) reveal that crack branching and subsequent growth can occur along one of the shear bands. The change in crack growth plane and branching due to a single overload are also evident from the scanning electron fractograph of Katz et al (34) for underaged 7075 aluminum alloy, shown in Fig. 3a and from the crack profiles obtained by Bucci et al (29) for overaged 7075-T7 alloy, shown in Fig. 3b. As the crack tends to propagate along the shear band, the change in crack growth direction (Fig. 2c) and the enhanced residual compressive stresses generated by the overload cycle significantly diminish the effective crack tip stress intensity range. Reports of various independent studies (19,21,29,33,35) have indicated that such reductions in ΔK_{eff} in the post-overload zone may result in an *effective* driving force comparable to the threshold stress intensity range for crack growth ΔK_0 , even though nominally higher baseline cyclic loads are applied externally. Contributions to reduction in stress intensity range due to crack branching and residual compressive stresses are estimated as follows.

3.1 RETARDATION DUE TO CRACK BRANCHING

An examination of existing information on crack tip profiles following overloads (19,29,33-35) indicates that the pre-overload crack can be "kinked" or "forked" due to the application of a single tensile overload. Such changes in crack geometry are schematically illustrated in Fig. 4. For a branched (or kinked) crack (Fig. 4a),

the Mode I and Mode II stress intensity factors, k_1 and k_2 , respectively, can be expressed as functions of the stress intensities for the main crack, K_1 and K_2 , such that

$$k_1 = \kappa_{11}(\theta) K_1 + \kappa_{12}(\theta) K_2 \quad (2)$$

$$k_2 = \kappa_{21}(\theta) K_1 + \kappa_{22}(\theta) K_2 \quad (3)$$

where θ is the angle denoting the extent of crack branching. Using typical values of $\theta = 45^\circ$ (Fig. 4a and ref. 29,33,35) and noting that $K_2 = 0$, the constants κ_{ij} can be obtained from the conformal mapping analyses of Bilby et al (36) for a semi-infinite crack with a kink of unit length at its tip (Table I). The stress intensity factors k_1 and k_2 are found to be $0.8 K_1$ and $0.3 K_1$, respectively, from eqns (2) and (3) and the effective stress intensity at the tip of the branched crack is

$$k = \sqrt{k_1^2 + k_2^2} \quad (4)$$

with the above calculations yielding $k = 0.85 K_1$. Such stress intensity estimates for kinked cracks, using an alternative method suggested by Kitagawa et al (37,38), lead to an effective stress intensity $k = 0.81 K_1$, for $b/a = 0.01$ in Fig. 4a. Thus it is seen that crack branching arising from a single overload could result in a reduction in effective stress intensity of up to 19%. In situations where the main crack is "forked" as a result of an overload (Fig. 4b and Fig. 2c), the decrease in driving force can be estimated, using similar analyses by Bilby et al (36) and Kitagawa et al to be about 35% of K_1 (assuming equal crack length on either side of the fork) (Table I).

As the kinked or forked crack branches out along one of the shear bands (29,33-35), it tends to change direction on intersecting a grain boundary and on trying to orient itself along the pre-overload main crack (33,35) (Fig. 2c). As such additional changes in crack growth direction occur (denoted by A in Fig. 2c), the effective stress intensity is even further reduced. A schematic illustration of such "doubly-kinked" crack is given in Fig. 4c. The stress intensity factors k_1 and k_2 at the tip of a doubly-kinked crack can be calculated using the expressions (39)

$$k_1 = K_1 \left\{ \cos^3\left(\frac{\theta}{2}\right) \cos^3\left(\frac{\alpha}{2}\right) + 3 \sin\left(\frac{\theta}{2}\right) \cos^2\left(\frac{\theta}{2}\right) \sin\left(\frac{\alpha}{2}\right) \cos^2\left(\frac{\alpha}{2}\right) \right\} \quad (5)$$

$$k_2 = K_1 \left\{ \cos^3\left(\frac{\theta}{2}\right) \sin\left(\frac{\alpha}{2}\right) \cos^2\left(\frac{\alpha}{2}\right) - \sin\left(\frac{\theta}{2}\right) \cos^2\left(\frac{\theta}{2}\right) \cos\left(\frac{\alpha}{2}\right) \right. \\ \left. [1 - 3 \sin^2 \frac{\alpha}{2}] \right\} \quad (6)$$

where θ and α are the angles representing the extent of the first and second kinks in crack path, respectively. Choosing typical values of $\theta = 45^\circ$ and $\alpha = 90^\circ$ (from Fig. 2c) for an aluminum alloy, k_1 and k_2 are found, as shown in Table I, to be about $0.63 K_1$ and $0.39 K_1$, respectively, such that the effective k at the tip of the doubly-kinked crack is estimated (using eq. 4) to be $0.74 K_1$.

The above model analyses, substantiated with experimentally observed crack tip profiles, clearly indicate that crack branching accompanying an overload cycle can result in pronounced reductions in the driving force. The type and extent of crack branching depend strongly on the

overload ratio r_{OL} , baseline stress intensity range ΔK_B and the alloy system (29,33). (It appears, from the information available in the literature (e.g. ref. 29), that crack branching is more significant at higher values of r_{OL} and lower ΔK_B and occurs only above a certain threshold r_{OL}). Moreover, the applied load is effectively lowered at the tip of a branched crack during the entire fatigue cycle, and the Mode II sliding accompanying crack branching also enhances the closure stress level. It should be noted that the above approximate analyses of stress intensity factors were obtained, ignoring the effects of the enlarged plastic zone generated by the overload.

3.2 RETARDATION DUE TO PLASTICITY EFFECTS

Plasticity-induced crack closure is generally considered to occur *in the wake* of the crack front due to the interference of the fractured faces even at positive loads as a result of the residual tensile displacements generated by crack tip plasticity (1,2). Such effects, which are known to be of significance under plane stress conditions (11,15), have been examined experimentally (11-15), analytically (40), and numerically (41). There is presently some controversy as to the applicability of plasticity-induced crack closure to plane strain loading situations (15). An important contribution to the above phenomenon can be considered to arise from the residual compressive stress field which exists *ahead* of the crack tip (5-7,42), within the cyclic plastic zone following unloading from a peak overload tensile stress. Since the baseline lower stress intensity range ΔK_B does not obliterate the enlarged cyclic plastic zone generated by the overload,

such residual compressive stresses due to the overload will act to close the crack during subsequent baseline cycling. Rice's plastic superposition analysis (5) of loading and unloading stress distributions for an elastic-perfectly plastic material stressed in fatigue reveals that the residual compressive stresses, σ_R (equal in magnitude to the flow stress in compression, $-\sigma_0$), act over a distance comparable to the extent of the cyclic plastic zone size, r_c , as shown in Fig. 5a. As the post-overload retarded crack progresses through the cyclic plastic zone generated by the overload, the residual stresses partially load the crack. A simple analysis to estimate the *maximum* reduction in effective driving force due to residual compressive stresses can be carried out by considering that a portion of the crack is loaded by a uniform stress σ_R ($= -\sigma_0$) over a distance $\rho \sim r_c$, as the post-overload crack traverses through the residual stress field, as shown in Fig. 5b. The stress intensity factor K_{1R} for this partially loaded crack is found from the analysis of Tada et al (43) to be

$$K_{1R} = \frac{2\sqrt{2}}{\sqrt{\pi}} \sigma \sqrt{\rho} \quad (7)$$

for $\rho \ll 2H$, the height of the specimen and $\rho \ll a$, the crack length. With $\sigma_R = -\sigma_0$ and $\rho \sim r_c$ and noting that the maximum extent of the cyclic plastic zone generated by a single overload of stress intensity range ΔK_{OL} is (44)

$$r_c = \frac{1}{2\pi} \left(\frac{\Delta K_{OL}}{2\sigma_0} \right)^2 \quad (8)$$

an expression for the stress intensity factor K_{1R} due to residual compressive stresses alone can be obtained. For positive values of the nominal load ratio R , the effective stress intensity range in the presence of enhanced residual stress field generated by the overload can be expressed, using linear superposition, as

$$\left[\Delta K_{\text{eff}} \right]_{R,OL} = K_{1\text{max}} + K_{1R,OL} \quad \text{when} \quad |K_{1R,OL}| \geq |K_{1\text{min}}| \quad (9)$$

since the effective $K_{1\text{min}}$ is zero when $|K_{1R,OL}| \geq |K_{1\text{min}}|$ and

$$\left[\Delta K_{\text{eff}} \right]_{R,OL} = K_{1\text{max}} - K_{1\text{min}} \quad \text{when} \quad |K_{1R,OL}| < |K_{1\text{min}}| \quad (10)$$

since residual compressive stresses are active during the complete loading cycle. Combining eqns. (7)-(9), the effective stress intensity range in the post-overload zone (taking into account only the effect of residual stresses) can be written as

$$\left[\Delta K_{\text{eff}} \right]_{R,OL} = K_{1\text{max}} - \frac{\Delta K_{OL}}{\pi} \quad \text{when} \quad |K_{1R,OL}| > |K_{1\text{min}}| \quad (11)$$

Residual compressive stresses are present even during constant amplitude loading and the effective stress intensity range in the presence of compressive stresses at pre-overload baseline ΔK_B has been obtained using similar analyses (45). In somewhat simplistic terms, this has been effectively modelled (45) using Irwin's physically-adjusted crack length concept and plastic zone (cyclic) such that

$$\left[\Delta K_{\text{eff}} \right]_{R,B} = K_{1\text{max}} - \frac{\Delta K_B}{\pi} \quad \text{when} \quad |K_{1R,B}| \geq |K_{1\text{min}}| \quad (12)$$

Thus the excess reduction in effective alternating stress intensity, $[\Delta K_{red}]_{R,OL}$ due to an enhanced residual stress field arising from a single overload can be calculated by subtracting eq. (11) from eq. (12), such that

$$[\Delta K_{red}]_{R,OL} = \frac{\Delta K_{OL} - \Delta K_B}{\pi} = \frac{K_{I\max}}{\pi} (r_{OL} - 1) \quad (13)$$

when $|K_{IR,OL}|$ and $|K_{IR,B}|$ are larger than $|K_{I\min}|$.

An examination of equations (9) through (13) reveals that residual compressive stresses play a major role in crack growth retardation only at lower nominal baseline load ratio (R) values. In other words, when $|K_{IR,OL}| < |K_{I\min}|$, the effective stress intensity range becomes equal to the nominal applied ΔK . It means that there is a critical *nominal* value of baseline load ratio, $R_{cr,OL}$ above which residual compressive stresses may not influence post-overload growth rates. This critical value of load ratio can be estimated by setting

$$|K_{IR,OL}| = |K_{I\min}| \quad (14a)$$

and noting that $\Delta K_{OL} = r_{OL} K_{I\max} - K_{I\min}$, such that

$$R_{cr,OL} = \frac{r_{OL}}{\pi + 1} \quad (14b)$$

Similarly, residual compressive stresses decrease the driving force during constant amplitude loading (45) only below a critical (nominal) load ratio, $R_{cr,B}$

$$R_{cr,B} = \frac{1}{\pi + 1} \quad (14c)$$

The above simple analyses have been found to be consistent with a number of experimental observations cited in the literature. Actual measurements of strain fields near the crack tip using stereoimaging techniques (46) do indeed reveal that the role of compressive stresses is much smaller following an overload at $R = 0.62$ than those for $R = 0.27$, in accordance with eqns. (9), (10) and (14b). In addition, the pronounced effects of residual compressive stresses in reducing effective ΔK only at low load ratios even in constant amplitude loading (eqns. 12) and (14c), and the values of $R_{cr,B}$, as predicted by the above analyses, are corroborated by results on effective driving force in a wide range of aluminum and ferrous alloys (11,21,29,45) at low stress intensity values.

Thus, the above models indicate that residual compressive stresses and crack branching could substantially reduce the effective ΔK responsible for crack advance in the post-overload zone. However, as discussed earlier, these two processes do not completely account for all the retardation effects following overloads. It therefore, becomes apparent that *additional* mechanistic possibilities should be considered in order to gain an understanding of the different transient effects due to load excursions.

Estimation or measurements of the actual driving force in the post-overload zone have shown that the *effective* stress intensity range at the crack tip could be close to the value of the threshold stress intensity factor range, ΔK_0 for fatigue crack growth despite a higher *nominal* post-overload ΔK_B (19,21,29,33,35). In other words, residual compressive stresses and crack branching could lower the effective stress intensity range to such an extent that near-threshold conditions

(Stage I growth in Forsyth's terminology (25)) exist effectively at the post-overload crack tip even though intermediate stress intensity conditions (Stage II growth in Forsyth's terminology (25)) are applied externally (16). While it is widely acknowledged that Stage II crack growth occurs by a striation mechanism induced by concurrent or alternating slip systems (25,28), Stage I (near-threshold) crack advance is known to take place primarily along a single slip system (25,48-50) since the plastic zone size generated by the *local* driving force is typically smaller than a grain size, as shown in Figs. 6a and 6d. Experimental evidence based on crack path and fractography in steels (Figs. 6b and 6e) (48), and in aluminum (Figs. 6c and 6f) (51,52) and titanium (53) alloys indicates that such Stage I propagation mechanism results in serrated or faceted fracture features and an irregular surface morphology and is accompanied by a strong Mode II displacement even under nominally Mode I cycling conditions. The occurrence of Mode II displacements during post-overload cycling and in near-threshold constant amplitude fatigue crack propagation has been verified experimentally using in-situ SEM analyses and from crack profiles showing the relative movement of the two fracture surfaces along the crack plane (33,35,50, 53,54). The presence of Mode II displacements and microscopically "rough" surface features (which clearly show the mechanistic similarities between constant amplitude near-threshold and post-overload crack advance) readily provide a mechanism for a reduction in effective ΔK due to premature contact of the fracture surfaces (16), in addition to the already discussed decrease in effective ΔK arising from crack branching and residual stresses. The extent of retardation due to "micro-roughness" is estimated in the following section.

3.3 MICRO-ROUGHNESS MODEL FOR CRACK GROWTH RETARDATION

Fracture surface micro-roughness is two-dimensionally modelled in terms of asperities assumed to be of triangular cross section and approximately equal in size (50), as shown in Fig. 7. Asperities have an average height h , base width w and semi-cone angle ψ at the tip. Fig. 7a shows the crack opening displacement δ_{1max} at the maximum load in the fatigue cycle. During the decreasing part of the loading cycle, the crack is assumed to be unloading in Mode I with a concomitant Mode II displacement (U_{II}) taken as a fraction x of the Mode I displacement (U_I). Then, the two fracture surfaces will first come into contact at a crack opening displacement of $\delta_{c1} = \delta_{1max} - U_I$ (Fig. 7a). Based on simple geometric considerations (as detailed in Fig. 7), the following expressions for closure and effective stress intensity factors, $K_{c1,MR}$ and $\Delta K_{eff,MR}$, respectively, due to premature contact of the fracture surfaces can be obtained;

$$\left[\frac{K_{c1}}{K_{1max}} \right]_{MR} = \sqrt{\frac{2\gamma x}{1+2\gamma x}} \quad (15)$$

$$\Delta K_{eff,MR} = K_{1max} \left[1 - \sqrt{\frac{2\gamma x}{1+2\gamma x}} \right] \quad (16)$$

where γ is a non-dimensional surface roughness parameter equal to h/w . The non-dimensional closure stress intensity factor $(K_{c1}/K_{1max})_{MR}$ is plotted in Fig. 7b as a function of γ to show the effect of micro-roughness for different values of x . With typical estimates of post-overload values $\gamma = 0.5$ and $x = 0.5$ for a 6061-T6 aluminum alloy (33), it is found from eqns. (15) and (16) that the closure stress intensity levels are about one third of the K_{1max} value. Note that this micro-roughness

induced retardation will be effective only if $\delta_{1min} < h$, where δ_{1min} is the minimum crack tip opening displacement.

From the above analysis and example, it is obvious that significant reductions in effective stress intensity range are caused by fracture surface microroughness and post-overload Mode II displacements. Thus, the micro-roughness model provides a new mechanistic basis for sustained retardation even when residual compressive stresses are not important, i.e., when retardation occurs well beyond the cyclic plastic zone generated by the overload (19,20,33,35,47). It should be noted that the micro-roughness mechanism *does not initiate* the process of retardation following an overload, but only *prolongs* crack growth attenuation once Stage I fatigue mechanisms are activated in the post-overload zone by residual compressive stresses, crack branching, and possibly some contribution from Elber-type closure in the wake of the advancing crack front. (Although fracture surface roughness along with Mode II displacements leads to crack face contact and hence closure, such closure processes are completely different from the mechanism of plasticity-induced crack closure originally proposed by Elber (1,2)). After the lowest crack propagation rate, as the retarded crack grows away from the zone of residual compressive stresses and crack branching (perturbations in crack path), a progressive increase in effective ΔK and lower Mode II displacements and abrasion result until the plastic zone size generated by the effective driving force roughly equals the grain size and the growth rates catch up with the nominal pre-overload baseline values.

An estimate of the extent of reduction in effective ΔK due to crack branching, residual compressive stresses and micro-roughness

can be obtained (as detailed in Table II) by considering the 6061-T6 aluminum alloy system shown in Fig. 2. From eqns. (5) and (6) and from the information in Fig. 2c, it is noted that crack branching alone results in a decrease in effective stress intensity of up to 26%. Moreover, the enlarged residual compressive stresses generated by the overload are found, from eqn. (13), to reduce the effective ΔK further by 32%. Thus crack branching and compressive stresses bring the effective ΔK down to $4.2 \text{ MPa}\sqrt{\text{m}}$ at the crack tip, (assuming concurrent action by the two processes) although the nominal $\Delta K_B = 10 \text{ MPa}\sqrt{\text{m}}$. The micro-roughness mechanism activated by such low effective ΔK values lowers the crack tip effective driving force by an additional 33% (as estimated from eqns. (15) and (16) with estimated values of $\gamma = 0.5$ and $x = 0.5$ for 6061-T6 aluminum alloy from ref. 33). This results in a predicted effective stress intensity range in the post-overload region of $2.8 \text{ MPa}\sqrt{\text{m}}$ (as summarized in Table II), even though the nominal ΔK_B is $10 \text{ MPa}\sqrt{\text{m}}$. Actual measurement of the effective stress intensity range for 6061-T6 aluminum alloy following a single overload (for the conditions used in Fig. 2, Table II and the present calculations) by Lankford and Davidson (33) have yielded a value of $\Delta K_{\text{eff}} = 2.2 \text{ MPa}\sqrt{\text{m}}$, in good agreement with the predictions of the above models.

4. SUPPORTING EVIDENCE AND IMPLICATIONS

The above models and mechanistic arguments for crack growth retardation, based on residual compressive stresses, crack branching and micro-roughness, rationalize a number of typical post-overload experimental observations related to mechanical, micro-structural and

environmental effects. Implications of the present interpretations and existing evidence in support of them are discussed in this section.

4.1 STRIATIONLESS POST-OVERLOAD CRACK ADVANCE

It has been found from several investigations (3,19,22-24,26, 28,29,34,47) that the application of a peak tensile overload could result in striationless crack growth in the post-overload region even for nominally Stage II loading conditions. Although attempts have been made to interpret such transient characteristics based on plasticity-induced crack closure concepts (3,22), such a behavior is fully consistent with the present argument that near-threshold (Stage I, single slip) mechanisms could *effectively* govern retarded crack advance following an overload, even though *nominally* Stage II conditions are expected. The presence of Mode II displacements, typical of Stage I growth (48-50), which have been experimentally confirmed for post-overload retarded crack propagation (33,35,46), corroborate the validity of such mechanistic interpretations.

4.2 FRACTURE SURFACE ABRASION FOLLOWING AN OVERLOAD

As mentioned earlier, it is a well documented observation that severe abrasion between the crack faces occurs in the post-overload zone (3,19,22-24, 26,28,29,34,47). Fig. 8 shows the fracture surface appearance due to pre-overload crack growth by a striation mechanism (region A), the stretch zone created by a single overload (region B), and the abrasion and serrated crack growth following an overload (region C), from ref. 22. The micro-roughness model readily provides a physically

appealing rationale for the occurrence of such abrasion in the post-overload zone since the Mode II displacements lead to asperity contact and cause "rubbing" and "relative sliding" between the crack faces (3,23). In situations where the overload is small ($\gamma_{OL} \lesssim 0.5$) and the ΔK_B values are high, striations are observed in the post-overload zone. Such a behavior is consistent with the present model because near-threshold conditions and Stage I crack advance cannot be initiated by small reductions in effective driving force at high ΔK_B values.

4.3 MICROSTRUCTURE-SENSITIVE RETARDED CRACK GROWTH

The post-overload crack propagation behavior is found to be influenced by microstructure as well as crack tip/grain boundary interactions (19,33,47), whereas Stage II constant amplitude crack advance at the same nominal ΔK_B is generally considered to be independent of microstructure (49). As it is known that Stage I crack propagation is highly microstructure sensitive (49,50), similar behavior in the post-overload zone is to be expected if the retarded crack is controlled by the micromechanisms of such Stage I growth, as detailed in this work.

4.4 DELAYED RETARDATION

Reductions in effective ΔK induced by micro-roughness and Mode II displacements sustain retardation once Stage I growth conditions are activated by other mechanisms such as residual compressive stresses and crack branching. The fact that events such as crack branching, lowering of the effective ΔK to near-threshold levels and initiation of Mode II displacements have to occur before growth rates are further

reduced by premature contact between the fracture surfaces, is consistent with the phenomenon of delayed retardation.

4.5 ENVIRONMENTAL EFFECTS ON CRACK GROWTH RETARDATION

Although the effects of mechanical and metallurgical factors on transient behavior following load excursion have been experimentally investigated in several studies (1-24,26-35), the important role of environment has received little attention. It has been shown that in some aluminum alloys, delay effects following overloads may be less pronounced in an aggressive environment compared to an inert gaseous environment, possibly due to the embrittling effect of the medium (20). As it is known that in moist environments, enlarged corrosion products formed on fracture surfaces due to fretting and rubbing at low growth rates can result in *additional* crack closure (29,55-58), the role of such additional closure processes is found to be a strong function of alloy composition and heat treatment in aluminum alloys (59,60). The corrosion products formed on the fracture surfaces of ASTM 7010-T7 aluminum alloy (29) during post-overload cycling are shown in Fig. 9a. A high magnification picture of the oxide layers formed during post-overload fatigue cycling in an ASTM A 542 class 3 steel are shown in Fig. 9b. Such excess corrosion layers formed due to fretting and rubbing contact between the two fracture surfaces following overload cycling are similar to those observed for near-threshold crack growth (57) and give further supporting evidence to the present argument that the micromechanisms of retarded crack growth due to load excursions are the same as those for near-threshold crack advance. Quantitative

estimates of the thickness of corrosion products in the post-overload region using scanning Auger spectroscopic analyses (16,57,58) show that the extent of oxidation due to fretting and rubbing in the retarded crack growth region could be higher (depending on r_{OL} and ΔK_B) than that for the same ΔK_B before the overload. Similar results have been obtained for a 2020 aluminum alloy (61) where the application of single tensile overloads at intervals of 8000 cycles is found to increase considerably the fracture surface oxidation as compared to constant amplitude cycling at the same ΔK_B level.

4.6 TRANSIENT EFFECTS DUE TO VARIOUS TYPES OF LOAD INTERACTIONS

Although the mechanistic descriptions of crack growth retardation discussed thus far have centered around transient effects associated with single spike overloads, these arguments could be extended to other types of variable amplitude loading situations as well. For example, the retardation or crack arrest resulting from a high-low block loading sequence is found to be much greater than that observed for a single overload of equivalent r_{OL} (22,26,29). The fractographic features associated with high-low block loading in a 2024-T3 aluminum alloy are illustrated in Fig. 10, from the work of von Euw (22). While mechanisms such as closure in the *wake* of the crack and residual compressive stresses have been previously used to rationalize retardation following high-low block loading, the extent of abrasion, fracture surface roughness (Figs. 10a and 10b) and microstructure sensitivity in the retardation zone clearly suggest that the micro-roughness mechanisms also plays a significant role in sustaining crack growth

retardation.

In variable amplitude fatigue tests involving underloads (compressive overloads) application of an underload prior to a single overload does not have any effect on subsequent retardation whereas an underload following an overload tends to minimize retardation (26). The former behavior is generally considered to be due to the closure of the crack during the application of an underload which does not generate any residual stress fields at the crack tip. However, since an overload severely blunts the crack tip (Figs. 2b and 2c) (and since the crack tip remains blunted even after unloading from the peak overload stress), subsequent underload cycling causes little closure in the wake and hence could generate residual tensile stresses at the crack tip which nullify some of the beneficial retardation effects of the overload.

4.7 PLANE STRAIN CRACK ARREST DUE TO OVERLOADS

Although crack growth retardation under predominantly plane stress conditions has been dealt with in detail by numerous investigators, little information is currently available on the mechanisms of growth attenuation under plane strain conditions. Crack propagation data for single overload cycling are presented in this section for a low strength 2 1/4 Cr- 1 Mo Steel (ASTM A 542 Class 3) at low baseline ΔK levels where predominately plane strain conditions prevail. The fully bainitic steel (hereafter referred to as SA 542-3) has chemical composition and mechanical properties shown in Table III. Crack arrest resulting from the application of a 100% single overload ($r_{OL} = 2$) at ΔK_B values of 9.0 MPa \sqrt{m} and 8.5 MPa \sqrt{m} (just above the threshold stress intensity range $\Delta K_0 =$

7.7 MPa \sqrt{m}) are shown in Fig. 11a and 11b, respectively, for a testing frequency of 50 Hz and load ratio of 0.05 in an environment of room temperature moist air (30% RH). No crack growth was observed even after 30 hours of post-overload cycling at ΔK_B . Such results clearly indicate that in plane strain crack growth, even a single overload can completely arrest the crack and result in a "premature threshold" ΔK_0 (Fig. 11c). From eq. (14) it is noted that for both values of ΔK_B , crack branching alone could reduce the driving force to such an extent that the effective ΔK responsible for crack advance is below the threshold for crack growth, ΔK_0 (= 7.7 MPa \sqrt{m}). Since no crack propagation can occur for stress intensities below ΔK_0 , complete crack arrest takes place in both cases, as found in Fig. 11a and 11b.

Although care is normally taken to avoid any load excursions during near-threshold crack growth measurements, spike loads (or "overshoots") could sometimes occur during automated load-shedding or "parking" the test overnight. As shown in Fig. 11, such spike loading results in premature values of ΔK_0 (higher than the actual ΔK_0) and erroneous interpretations.

5. CONCLUSIONS

It is demonstrated with the aid of extensive experimental evidence from the literature that post-overload retarded crack advance is governed primarily by the micromechanisms of near-threshold crack growth. A new mechanism for enhanced retardation is suggested based on a micro-roughness model. It is reasoned that closure in the wake of the crack

tip due to residual tensile displacements is not likely to be the *primary* mechanism for retardation. Simple mechanical models are presented to show that substantial decrease in effective stress intensity range occurs due to crack branching, residual compressive stresses and fracture surface asperity contact following an overload. The predictions of such models are found to be in good agreement with the measured values of effective stress intensity in the post-overload zone. A number of mechanical, microstructural, and environmental phenomena typically observed after the application of an overload has been rationalized in terms of the present arguments. The importance of an understanding of such concepts to crack growth measurement and analysis is emphasized.

ACKNOWLEDGEMENTS

This work was supported by the Director, Office of Energy Research, office of Basic Energy Sciences, Materials Science Division of the U.S. Department of Energy under contract No. DOE-AC03-76SF00098. The author is grateful to Professor R. O. Ritchie for his continued support and encouragement. Many valuable suggestions and constructive criticisms from Professor A. G. Evans are also gratefully acknowledged.

REFERENCES

- (1) W. Elber, The Significance of fatigue crack closure, in Damage Tolerance in Aircraft Structures, ASTM STP 486, 230-242 (1971).
- (2) W. Elber, Fatigue crack closure under cyclic tension, Engng. Fract. Mech., 2, 37-45 (1970).
- (3) E. F. J. von Euw, R. W. Hertzberg and R. Roberts, Stress analysis and growth of cracks, ASTM STP 513, 230 (1972).
- (4) R.H. Christensen, Metal Fatigue, McGraw-Hill, New York (1959).
- (5) J. R. Rice, Mechanics of crack tip deformation and extension by fatigue, in Fatigue Crack Propagation, ASTM STP 415, 247-311. (1967).
- (6) J. Schijve, Fatigue crack propagation in light alloy sheet materials and structures, NRL report MP 195, Amsterdam, The Netherlands (1960).
- (7) C. M. Hudson and H. F. Hardrath, "Effects of changing stress amplitude on the rate of fatigue crack propagation of two aluminum alloys, NASA Technical Note D-960, (1961).
- (8) O. E. Wheeler, Spectrum loading and crack growth, J. Basic Engng., Trans. ASME, Series D, 94(1), 181-186 (1972).
- (9) J. Willenborg, R. M. Engle and H. A. Wood, A crack growth retardation model using an effective stress intensity concept, Technical Report TFR 71-701, Los Angeles Division, North American Rockwell (1971).
- (10) R. E. Jones, Fatigue crack growth retardation after single cycle peak overload in Ti-6Al-4V titanium alloy, Engng. Fract. Mech., 5, 585-604 (1973).
- (11) J. F. Knott and A. C. Pickard, Effects of overloads on fatigue crack propagation: aluminum alloys, Met. Science, 11, 399-404 (1977).
- (12) G. Marci and P. F. Packman, The effects of plastic wake zone on the conditions for fatigue crack propagation, Int. J. Fract., 16, (1980).
- (13) D. Broek and J. Schijve, NRL Report TRM2119, The Netherlands (1963).
- (14) T. C. Lindley and C.E. Richards, The relevance of crack closure to fatigue crack propagation, Mater. Sci. Engng., 14, 281-293 (1974).
- (15) A. J. McEvily, Current aspects of fatigue, Met. Science, 11, 274-284 (1977).

- (16) S. Suresh, Crack growth retardation due to micro-roughness: A mechanism for overload effects in fatigue, *Scripta Met.*, 16, No. 8, (1982).
- (17) H. F. Hardrath and A. J. McEvily, Proceeding of the Crack Propagation Symposium, Vol. 1, Cranfield, England (1961).
- (18) D. Broek, Elementary engineering fracture mechanics, Noordhof (1978).
- (19) G. R. Chanani, Effect of thickness on retardation behavior of 7075 and 2024 aluminum alloys, in *Flaw growth and fracture*, ASTM STP 631, 365-387 (1977).
- (20) R. P. Wei, N. E. Fenelli, K. D. Unangst, and T. T. Shih, Fatigue crack growth response following a high-load excursion in 2219-T851 aluminum alloy, *J. Eng. Mat. Tech., Trans. ASME*, 102, 280-292 (1980).
- (21) P. J. Bernard, T. C. Lindley and C. E. Richards, The effect of single overloads on fatigue crack propagation in steels, *Met. Sci.*, 12, 390-398 (1977).
- (22) E. F. J. von Euw, Effect of overload cycle(s) on subsequent fatigue crack propagation in 2024-T3 aluminum alloy, Ph.D. Thesis, Lehigh University (1971).
- (23) R. W. Hertzberg, Deformation and fracture mechanics of engineering materials, 1st edn., John Wiley & Sons, New York (1976).
- (24) W. J. Mills, Load interaction effects on fatigue crack growth in 2024-T3 aluminum and A514F steel alloys, Ph.D. Thesis, Lehigh University (1975).
- (25) P. J. E. Forsyth, Crack propagation, Proceedings of Symposium, Cranfield, England (1961).
- (26) D. M. Corlby and P. F. Packman, On the influence of single and multiple peak overloads on fatigue crack propagation in 7075-T6511 aluminum, *Engng. Fract. Mech.*, 5, 479-497 (1973).
- (27) J. C. McMillan and R. M. N. Pelloux, Fatigue crack propagation under program and random loads, in *Fatigue crack propagation*, ASTM STP 415, 505-535 (1966).
- (28) R. M. N. Pelloux, Crack extension by alternating shear, *Engng. Fract. Mech.*, 1, 697-704 (1970).
- (29) R. J. Bucci, A. B. Thakker, T. H. Sanders, R. R. Sawtell, and J. F. Staley, Ranking 7xxx aluminum alloy fatigue crack growth resistance under constant amplitude and spectrum loading, in *Effect of load spectrum variables on fatigue crack initiation and propagation*, ASTM STP 714, 41-78 (1980).

- (30) O. Jonas and R. P. Wei, An exploratory study of delay in fatigue crack growth, *Int. J. Fract.*, 7, 116-118 (1971).
- (31) R. P. Wei and T. T. Shih, Delay in fatigue crack growth, *Int. J. Fract.*, 10(1), 77-85 (1974).
- (32) T. T. Shih and R. P. Wei, A study of crack closure in fatigue, *Engng. Fract. Mech.*, 6, 19-32 (1974).
- (33) J. Lankford and D. L. Davidson, The effect of overloads upon fatigue crack tip opening displacement and crack tip opening/closing loads in aluminum alloys, in *Advances in Fracture Research*, D. Francois et al, editors, vol. 2, Pergamon Press, 899-906 (1981).
- (34) Y. Katz, A. Bussiba and H. Mathias, Micromechanisms of fatigue crack growth exposed to load transient effects, *Met. Sci.*, 15, 317-319 (1981).
- (35) J. Lankford and D. L. Davidson, Fatigue crack tip plasticity associated with overloads and subsequent cycling, *J. Engng. Mat. Tech.*, *Trans. ASME*, 98, 17-23 (1976).
- (36) B. A. Bilby, G. E. Cardew and I. C. Howards, Stress intensity factors at the tip of kinked and forked cracks, in *Fracture 1977*, D. M. R. Taplin, ed., vol. 3, Univ. of Waterloo Press, 197-200 (1977).
- (37) H. Kitagawa and R. Yuuki, Analysis of branched cracks under biaxial stresses, in *Fracture 1977*, D. M. R. Taplin, ed., vol. 3, Univ. of Waterloo Press, 201-211 (1977).
- (38) H. Kitagawa, R. Yuuki and T. Ohira, Crack-morphological aspects in fracture mechanics, *Engng. Fract. Mech.*, 7, 515-529 (1975).
- (39) K. Faber, Toughening of ceramic materials by crack deflection processes, Ph.D. Thesis, University of California, Berkeley (1982).
- (40) B. Budiansky and J. W. Hutchinson, Analysis of closure in fatigue crack closure, *ASTM STP 590*, 281-300 (1974).
- (42) J. Tirosh and A. Ladelski, Note on residual stresses induced by fatigue cracking, *Engng. Fract. Mech.*, 13, 453-462 (1980).
- (43) H. Tada, P. C. Paris and G. R. Irwin, *Stress Analysis of cracks handbook*, Del Research Corp., Hellertown, Pennsylvania (1973).
- (44) C. F. Shih, Relationships between the J-integral and crack opening displacement for stationary and extending cracks, *J. Mech. Phys. Sol.*, 29, 305-330 (1981).
- (45) S. Suresh and R. O. Ritchie, A model for the contribution to plasticity-induced crack closure due to residual compressive stresses, *Mater. Sci. Engng.*, 55 (1982), in press.

- (46) D.L. Davidson and J. Lankford, Fatigue crack tip plasticity resulting from load interactions in an aluminum alloy, *Fat. Engng. Mater. Struct.*, 1, 439-446 (1979).
- (47) J. M. Baik, L. Hermann and R. J. Asaro, Fatigue crack growth and overload retardation in 2048 aluminum, in *Mechanics of fatigue*, T. Mura, ed., ASME, New York (1981).
- (48) K. Minakawa and A. J. McEvily, On crack closure in the near-threshold region, *Scripta Met.*, 15, 633-636 (1981).
- (49) R. O. Ritchie and S. Suresh, Some consideration on fatigue crack closure induced by fracture surface morphology, *Met. Trans.*, 13A, 937-940 (1982).
- (50) S. Suresh and R. O. Ritchie, A geometric model for fatigue crack closure induced by fracture surface roughness, *Met. Trans.*, 13A (1982), in press.
- (51) E. P. Louward, Delft Univ. of Tech., Dept. Aero. Eng. Report LR-243, The Netherlands (1977).
- (52) J. Schijve, in *Fatigue Thresholds*, Proc. 1st Intl. Conf., Stockholm, J. Backlund et al, eds., EMAS Publ. Ltd., Warley, U.K. (1982).
- (53) N. Walker and C. J. Beevers, A fatigue crack closure mechanism in titanium, *Fat. Engng. Mat. Struct.*, 1, 135-148 (1979).
- (54) D. L. Davidson, Incorporating threshold and environmental effects into the damage accumulation model for fatigue crack growth, *Fat. Engng. Mat. Struct.*, 3, 229-236 (1981).
- (55) R. O. Ritchie, S. Suresh and C. M. Moss, Near-threshold fatigue crack growth in 2½Cr-1Mo pressure vessel steel in air and hydrogen, *J. Engng. Mat. Tech.*, Trans. ASME, Series H, 102, 293-299 (1980).
- (56) A. T. Stewart, The influence of environment and stress ratio on fatigue crack growth at near-threshold stress intensities in low alloy steels, *Engng. Fract. Mech.*, 13, 463-478 (1980).
- (57) S. Suresh, G. F. Zamiski and R. O. Ritchie, Oxide-induced crack closure: An explanation for near-threshold corrosion fatigue crack growth behavior, *Met. Trans.*, 12A, 1435-1443 (1981).
- (58) S. Suresh, D. M. Parks and R. O. Ritchie, Crack tip oxide formation and its influence on fatigue thresholds, in *Fatigue thresholds*, Proc. First Int. Symp., A. F. Blom et al (eds). EMAS publishers, Warley, U.K. (1982) in press.

- (59) S. Suresh, I. G. Palmer and R. E. Lewis, The effect of environment on fatigue crack growth behavior of 2021 aluminum alloy, *Fat. Engng. Mat. Struct.*, 4 (1982) in press.
- (60) A. K. Vasudevan and S. Suresh, Influence of corrosion deposits on near-threshold fatigue crack growth behavior in 2xxx and 7xxx series aluminum alloys, *Met. Trans.*, 14A (1982) in press.
- (61) A. K. Vasudevan and P. E. Bretz, presentation at AIME Winter Annual Meeting, Dallas, 1982.

Table I
Stress Intensity Factor Calculations for Branched Cracks

<u>Type of Branching</u>	<u>Condition</u>	<u>k_1/K_1</u>	<u>k_2/K_1</u>	<u>k/K_1</u>	<u>Reference</u>
a) kinked crack (Fig. 4a) $\theta \approx 45^\circ$	$b \ll a$	0.8	0.3	0.85	(36)
	$b/a=0.01$	0.71	0.39	0.81	(37)
b) forked crack (Fig. 4b) $2\theta \approx 90^\circ$	$\left\{ \begin{array}{l} b \ll a \\ b \approx c \end{array} \right\}$	0.58	0.33	0.65	(36)
		0.6	0.3	0.67	(38)
c) doubly-kinked crack (Fig. 4c) $\theta \approx 45^\circ$ $\alpha = 90^\circ$	$\left\{ \begin{array}{l} b \ll a \\ \left[\begin{array}{l} b > c \\ \text{or } c = 0 \end{array} \right] \end{array} \right\}$	0.63	0.39	0.74	(39)

Table II

Comparison of Predicted and Measured Effective Intensity Range in the Post-Overload Region for the 6061-T6 Aluminum Alloy Shown in Fig. 2.

Loading Conditions: $\Delta K_B = 10 \text{ MPa}\sqrt{\text{m}}$; $r_{OL} = 1.8$; $R = 0.2$

Mechanism	Conditions	Equations	Result
a) Crack Branching	$\theta \approx 45^\circ$, $\alpha \approx 90^\circ$ $b \ll a$	(4)-(6)	$k/K_I \approx 0.74$ reduction in $\Delta K_{\text{eff}} \approx 0.25 \Delta K_B$
b) Crack-tip Plasticity	$\Delta K_B = 10 \text{ MPa}\sqrt{\text{m}}$ $r_{OL} = 1.8$ $R = 0.2$	(13)	$[\Delta K_{\text{red}}]_{R,OL} = 0.25 K_{I\text{max}}$ $\approx 0.32 \Delta K_B$ ($\because K_{I\text{max}} = \Delta K_B / (1-R)$)
Effective ΔK with the combined action of (a) and (b) is $[\Delta K]_{(a),(b)} \approx 0.42 \Delta K_B = 4.2 \text{ MPa}\sqrt{\text{m}}$			
c) Micro-Roughness and Mode II Effects	$x = 0.5$ $\gamma = 0.5$	(15) and (16)	$\Delta K_{\text{eff}} = 0.67 [\Delta K]_{(a),(b)}$

Predicted ΔK_{eff} in the post-overload region = $0.67 \times 4.2 \text{ MPa}\sqrt{\text{m}} = 2.8 \text{ MPa}\sqrt{\text{m}}$

Measured ΔK_{eff} in the post-overload region (from ref. 33) = $2.2 \text{ MPa}\sqrt{\text{m}}$

Table III
Chemical Composition and Mechanical Properties of SA 542-3 Steel

a) Chemical Composition (wt. pct.)

C	Mn	Si	Ni	Cr	Mo	P	S	Cu	Fe
0.12	0.45	0.21	0.11	2.28	1.05	0.014	0.015	0.12	Balance

b) Room Temperature Mechanical Properties

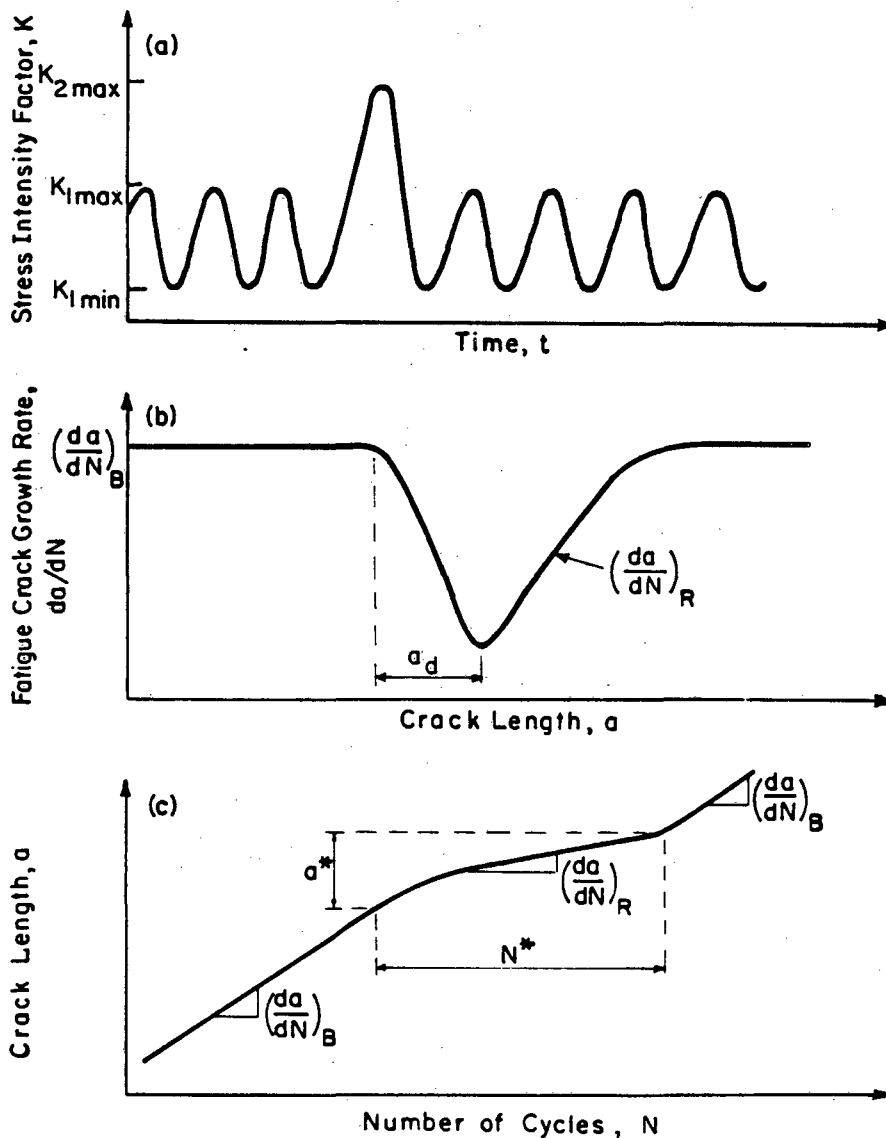
0.2% Offset Yield Strength		U.T.S.	Redn. in Area	K_{Ic}
<u>monotonic</u> (MPa)	<u>cyclic</u> (MPa)	(MPa)	(Pct)	(MPa \sqrt{m})
500	400	610	77	295

Nominal Load Ratio, $R = K_{1min}/K_{1max}$

Baseline Stress Intensity Range, $\Delta K_B = K_{1max} - K_{1min}$

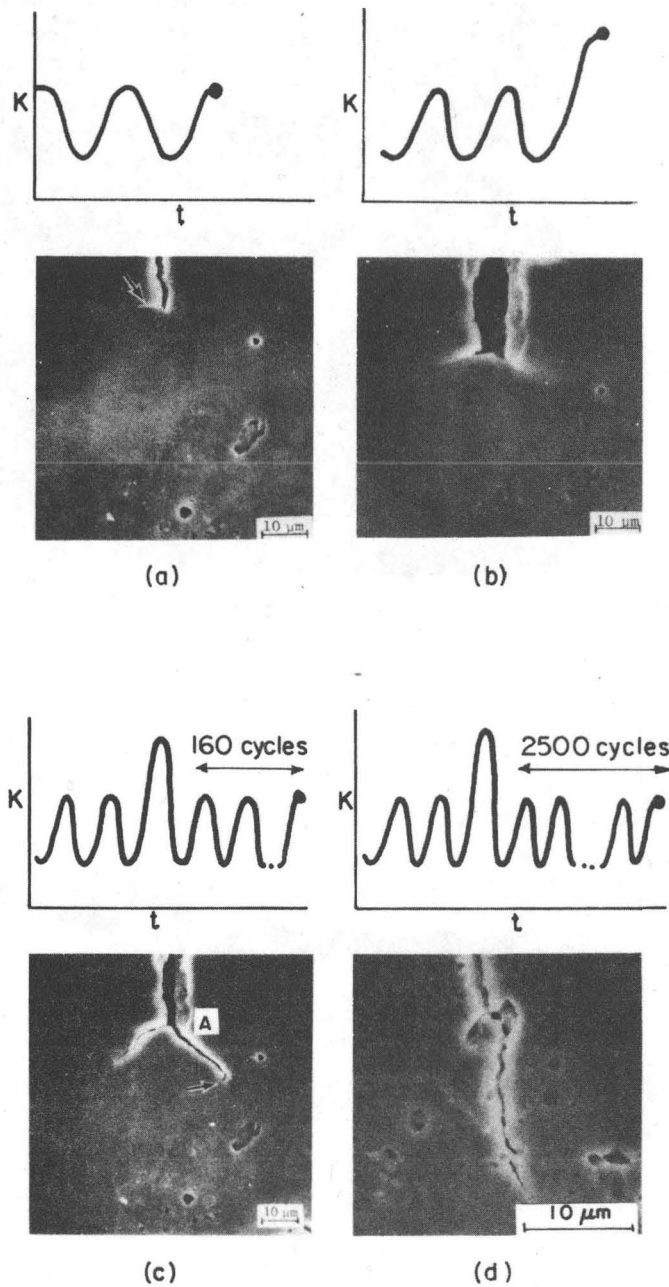
Overload Stress Intensity Range, $\Delta K_{OL} = K_{2max} - K_{1min}$

Overload Factor, $r_{OL} = K_{2max}/K_{1max}$



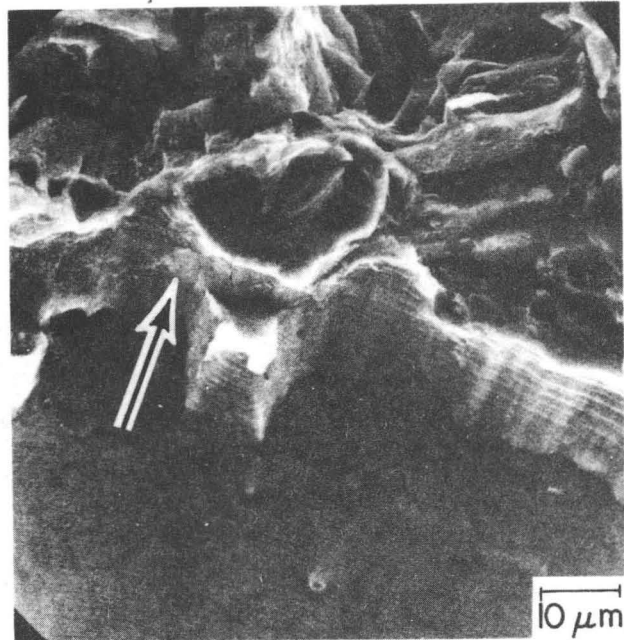
XBL 825-5717

Fig. 1 Nomenclature of different parameters used to describe overload interactions on fatigue crack growth.

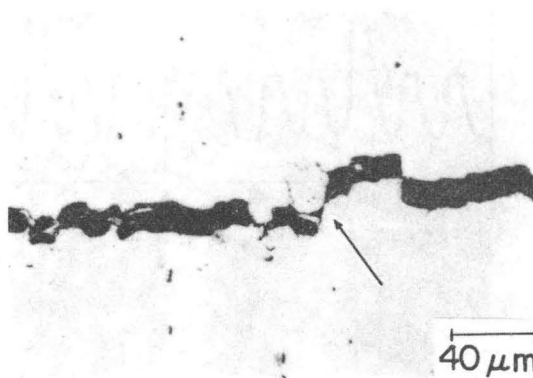


XBB 825-4826

Fig. 2 Sequential changes in crack profile due to an overload interaction in 6061-T6 aluminum alloy at $\Delta K_B = 10 \text{ MPa}\sqrt{\text{m}}$, $R \approx 0.2$ and $r_{OL} = 1.8$; (a) Pre-overload, $K = K_{1\text{max}}$; (b) overload, $K = K_{2\text{max}}$; (c) 160 cycles following an overload, $K = K_{1\text{max}}$ and (d) 2500 cycles following an overload, $K = K_{1\text{max}}$ (after ref. 33).



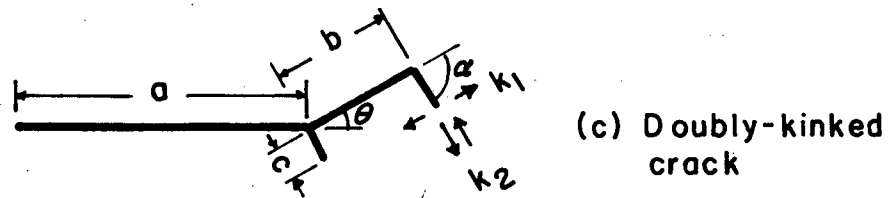
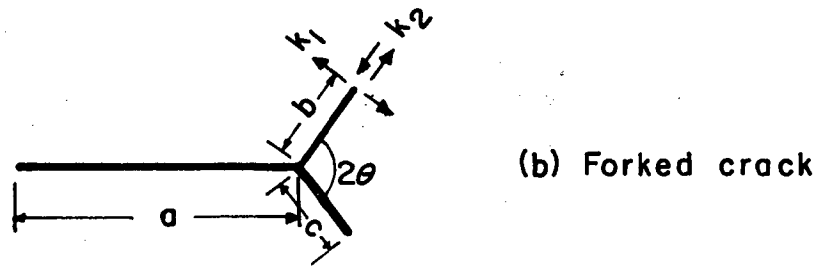
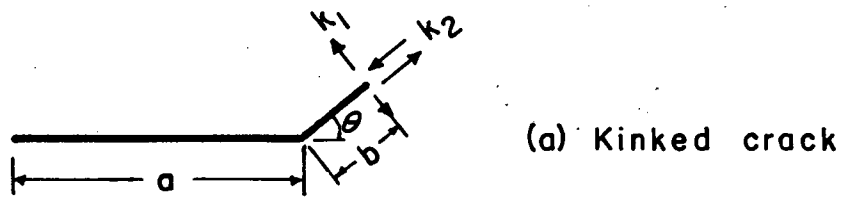
(a)



(b)

XBB 825-4846

Fig. 3. Changes in crack growth plane following an overload: (a) in underaged 7075 aluminum alloy (after ref. 34); arrow indicates crack growth direction; (b) in overaged 7075-T7 aluminum alloy (after ref. 29); arrow indicates the point of application of an overload.



XBL 826-5860

Fig. 4 Schematic showing possible types of crack branching after an overload and the corresponding nomenclature to describe stress intensity factors.

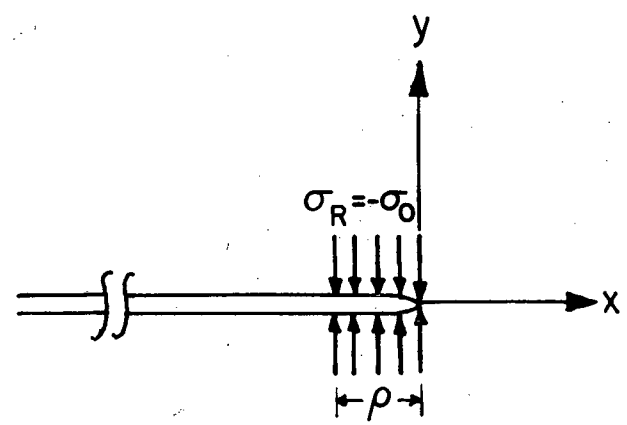
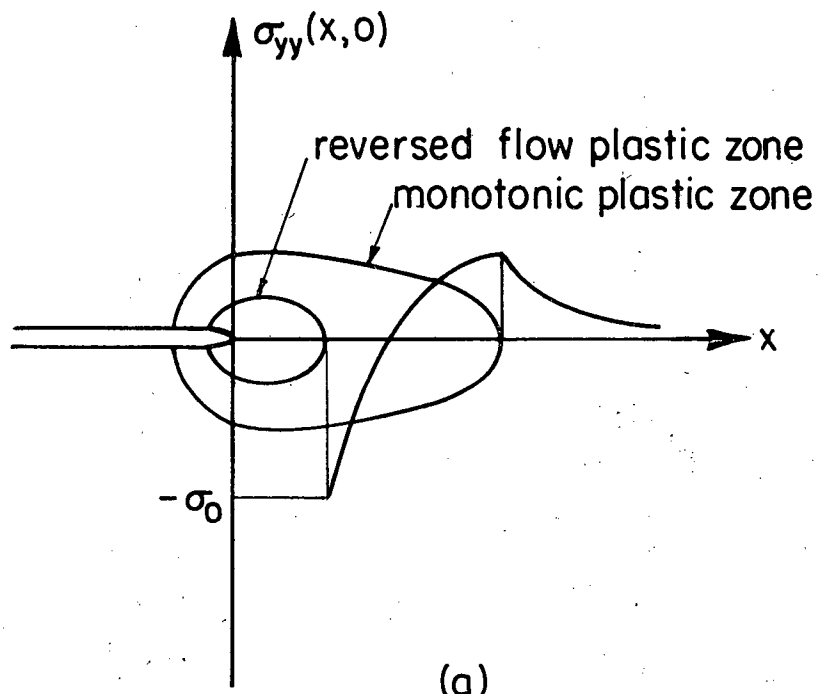


Fig. 5 Illustrations of plastic zones ahead of a fatigue crack where the maximum influence of the residual stresses is effectively modelled to be active over a distance $\rho \sim \gamma_C$, the enlarged cyclic plastic zone size, by partially loading the crack.

XBL 824-5538A

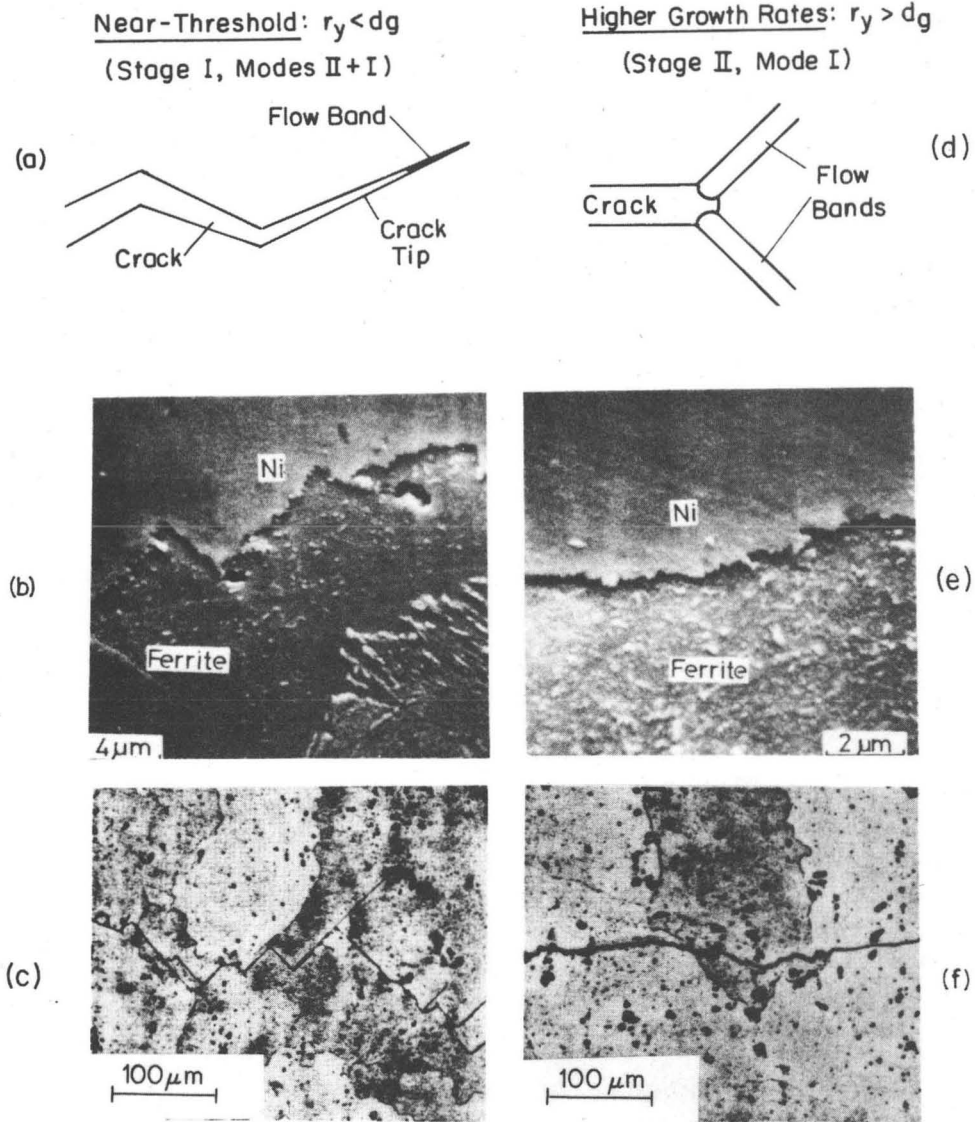
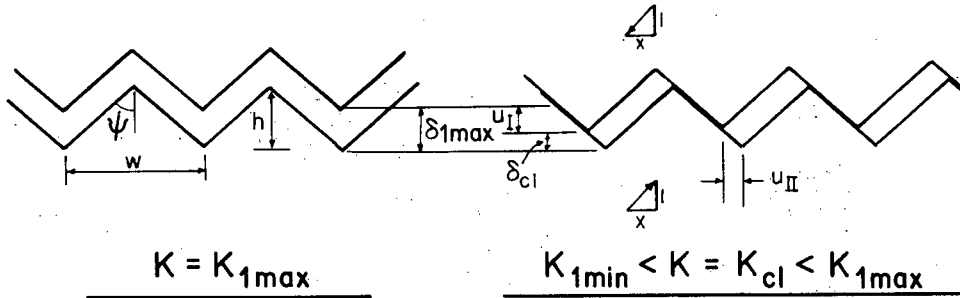
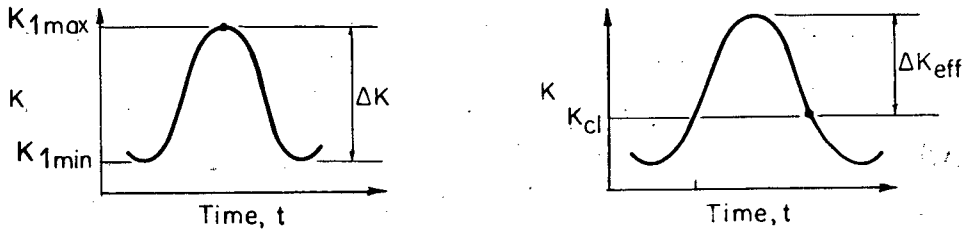


Fig. 6 Crack opening profiles and resulting crack path morphologies corresponding to (a), (b), (c) near-threshold (Stage I) and (d) (e) (f) higher growth rates (Stage II) fatigue crack propagation. (b) and (e) are nickel-plated fracture sections of fatigue crack growth in 1018 steel (after ref. 48) and (c) and (f) are metallographic sections of crack growth in 7075-T6 aluminum alloy (after ref. 51). r_y is the maximum plastic zone size and d_g the average grain size.



$$K = K_{1max}$$

$$K_{1min} < K = K_{cl} < K_{1max}$$

$$\delta_{cl} = \delta_{1max} - u_{II}$$

$$x = u_{II} / u_I$$

$$\cot \psi = h / (w/2) = \delta_{cl} / u_{II}$$

$$\delta_{cl} = \frac{2hx \delta_{1max}}{w + 2hx}$$

$$\frac{K_{cl}}{K_{1max}} = \sqrt{\frac{\delta_{cl}}{\delta_{1max}}} = \sqrt{\frac{2\gamma x}{1 + 2\gamma x}}$$

or in nondimensional form, with $\gamma = h/w$,

$$\left[\frac{K_{cl}}{K_{1max}} \right]_{MR} = \sqrt{\frac{2\gamma x}{1 + 2\gamma x}}$$

$$\left[\Delta K_{eff} \right]_{MR} = K_{1max} - K_{cl} = K_{1max} \left[1 - \sqrt{\frac{2\gamma x}{1 + 2\gamma x}} \right]$$

(a)

XBL 82I-5084A

Fig. 7 (a)

Fig. 7 (a) Schematic illustration of Stage I fatigue crack in the fully-open and unloading configurations and derivation of expression for K_{cl} and ΔK_{eff} accounting for fracture surface micro-roughness (50); (b) Variation of non-dimensional closure stress intensity $(K_{cl}/K_{1max})_{MR}$ with non-dimensional roughness parameter γ for different values of x .

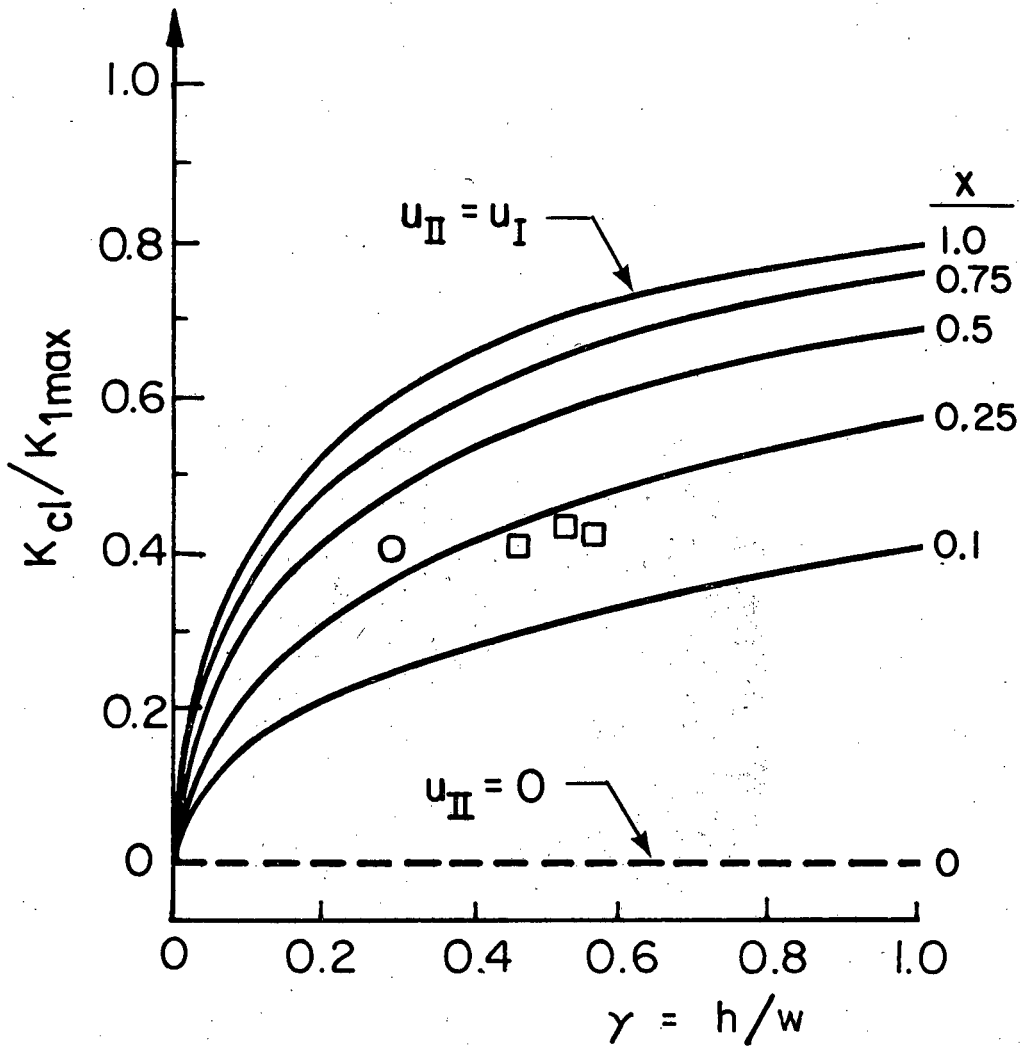
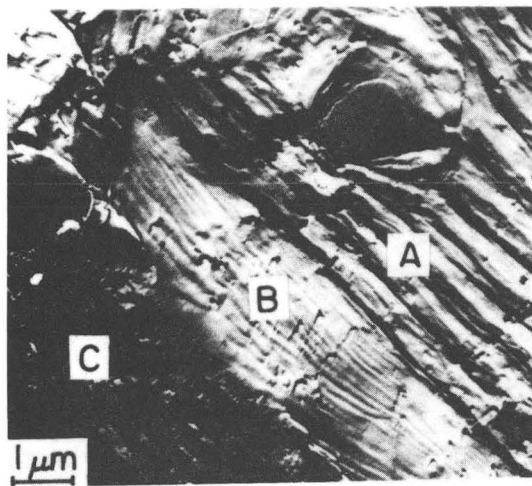


Fig. 7 (b)

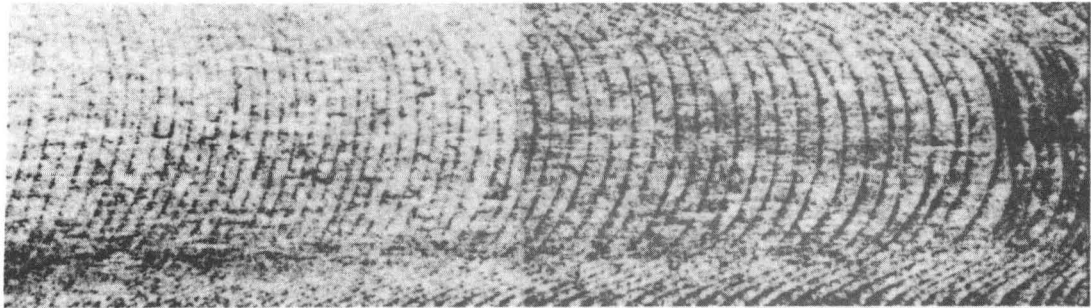
(b)

XBL 821-5083A

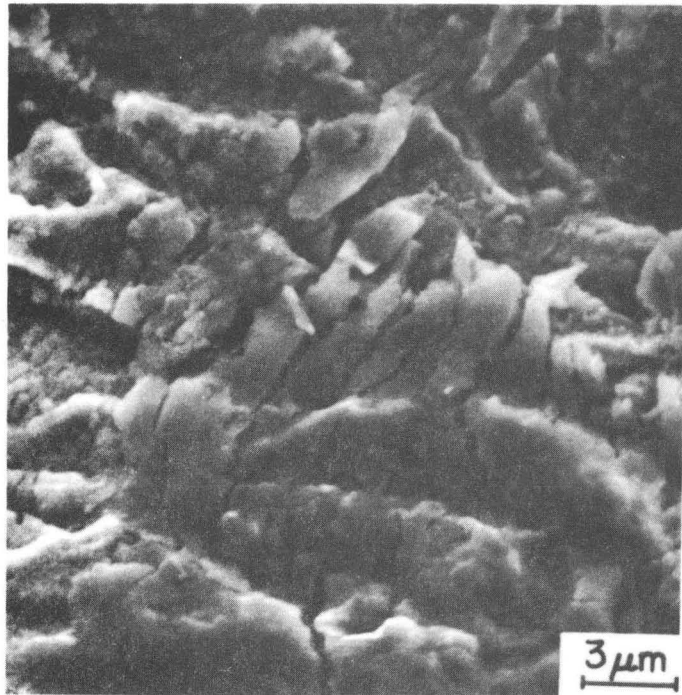


XBB 825-4847A

Fig. 8. Fractograph showing the surface appearance in the pre-overload zone (A), stretch zone (B), and the post-overload zone (C) in 2024-T3 aluminum alloy (after ref. 22).



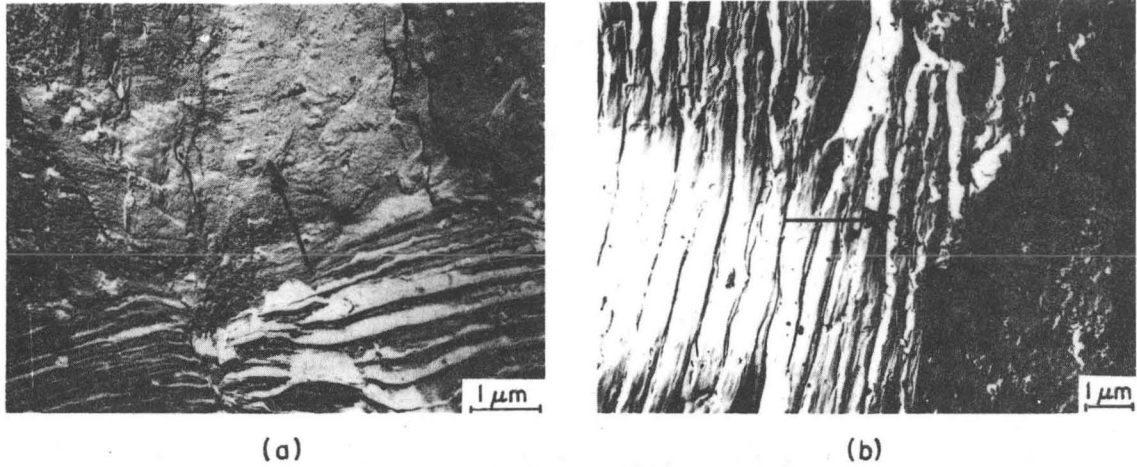
(a)



XBB 826-5019

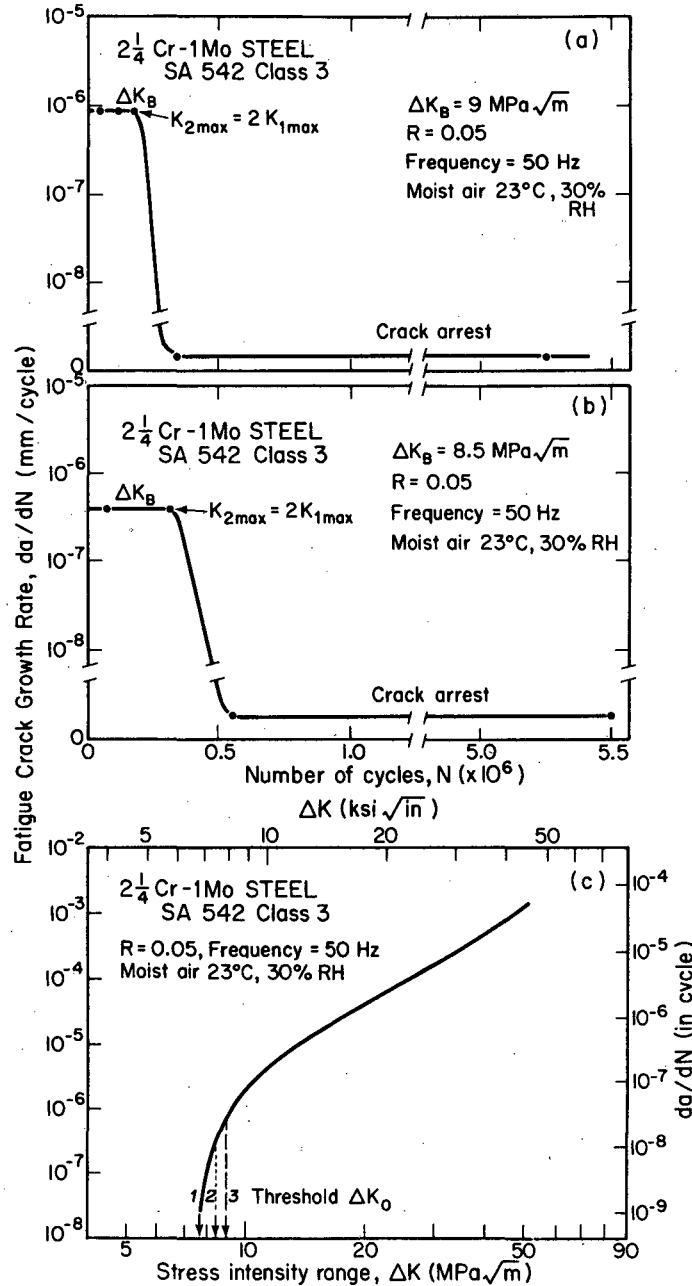
(b)

Fig. 9 Bands of corrosion products formed on the fracture surfaces due to fretting and rubbing following an overload in (a) 7010-T7 aluminum alloy (after ref. 29) and (b) SA542-3 steel (present study).



XBB 825-4825

Fig. 10 Fractographic features resulting from high-low block loading sequences in a 2024-T3 aluminum alloy (after ref. 22). (a) $\Delta K_B = 9.8 \text{ MPa}\sqrt{\text{m}}$ and $\Delta K_{OL} = 14.7 \text{ MPa}\sqrt{\text{m}}$; (b) $\Delta K_B = 16.4 \text{ MPa}\sqrt{\text{m}}$ and $\Delta K_{OL} = 24.5 \text{ MPa}\sqrt{\text{m}}$. Arrow indicates crack growth direction.



XBL 825-693

Fig. 11 Complete crack arrest following a single overload during plane strain crack growth in SA 542-3 steel (a) at $\Delta K_B = 9 \text{ MPa}\sqrt{\text{m}}$ and (b) at $\Delta K_B = 8.5 \text{ MPa}\sqrt{\text{m}}$. Fig. (c) shows the premature values of ΔK_0 obtained due to the application of a single overload at ΔK_B values of $9 \text{ MPa}\sqrt{\text{m}}$ (point 3) and $8.5 \text{ MPa}\sqrt{\text{m}}$ (point 2). Point 1 corresponds to the measured value of ΔK_0 with no overloads.

This report was done with support from the Department of Energy. Any conclusions or opinions expressed in this report represent solely those of the author(s) and not necessarily those of The Regents of the University of California, the Lawrence Berkeley Laboratory or the Department of Energy.

Reference to a company or product name does not imply approval or recommendation of the product by the University of California or the U.S. Department of Energy to the exclusion of others that may be suitable.

TECHNICAL INFORMATION DEPARTMENT
LAWRENCE BERKELEY LABORATORY
UNIVERSITY OF CALIFORNIA
BERKELEY, CALIFORNIA 94720